Estimation of secondary organic aerosol formation parameters for the Volatility Basis Set combining thermodenuder, isothermal dilution and yield measurements

Petro Uruci[1,2], Dontavious Sippial[3], Anthoula Drosatou[1,2], and Spyros N. Pandis[1,2]

[1]Institute of Chemical Engineering Sciences (FORTH/ICE-HT), 26504, Patras, Greece
[2]Department of Chemical Engineering, University of Patras, 26500, Patras, Greece
[3]Department of Chemical Engineering, Carnegie Mellon University, Pittsburgh, USA

Abstract

Secondary organic aerosol (SOA) is a major fraction of the total organic aerosol (OA) in the atmosphere. SOA is formed by the partitioning onto pre-existent particles of low vapor pressure products of the oxidation of volatile, intermediate volatility, and semivolatile organic compounds. Oxidation of the precursor molecules results in a myriad of organic products making the detailed analysis of smog chamber experiments difficult and the incorporation of the corresponding results into chemical transport models (CTMs) challenging. The volatility basis set (VBS) is a framework that has been designed to help bridge the gap between laboratory measurements and CTMs. The parametrization of SOA formation for the VBS has been traditionally based on fitting yield measurements of smog chamber experiments. To reduce the uncertainty of this approach, we developed an algorithm to estimate the SOA product volatility distribution, effective vaporization enthalpy, and effective accommodation coefficient combining SOA yield measurements with thermograms (from thermodenuders) and areograms (from isothermal dilution chambers) from different experiments and laboratories. The algorithm is evaluated with "pseudo-data" produced from the simulation of the corresponding processes assuming SOA with known properties and introducing experimental error. One of the novel features of our approach is that the proposed algorithm estimates the uncertainty of the predicted yields for different atmospheric conditions (temperature, SOA concentration levels, etc.). The uncertainty of these predicted yields uncertainty is significantly lesssmaller than that of the estimated volatility distributions for all conditions tested.
We show that even though there is still significant remaining uncertainty in the estimates (volatility distribution of the products and effective accommodation coefficient), the situation is dramatically better for the predicted yields at different atmospheric conditions.

Commented [ОП1]: Reviewer #3, Comment #7

Commented [ОП2]: Reviewer #3, Comment #8

Commented [ОП3]: Reviewer #2, Comment #21

1

1. Introduction

Submicrometer atmospheric particles are of great importance due to their negative effects on public health (Pope and Dockery, 2006; Lim et al., 2012) and their uncertain influence on Earth's climate (IPCC, ~~2013~~ 2021). Organic aerosol (OA) contributes 20–90 % to the submicron particulate mass (Zhang et al., 2007) and is emitted directly in the atmosphere as primary particles (POA) or formed as secondary organic aerosol (SOA). SOA constitutes a major fraction of the total OA in the atmosphere contributing more than 60 % on average (Kanakidou et al., 2005). SOA is formed by the condensation of low vapor pressure products of the oxidation of volatile (VOCs), intermediate volatility (IVOCs), and semi-volatile organic compounds (SVOCs).

Hundreds of mostly unknown products are formed during the oxidation of each SOA precursor making the detailed description of the corresponding reactions and eventual SOA formation extremely challenging. The volatility basis set (VBS) is one approach that has been proposed to simplify the system and to allow the SOA simulation in CTMs. The VBS describes the volatility distribution of OA using a set of surrogate species with effective saturation concentrations that vary by one order of magnitude (Donahue et al., 2006; Stanier et al., 2008). Volatility is one of the most important physical properties of SOA components as it determines to a large extent their gas-particle partitioning (Pankow, 1994a; 1994b). The parametrization of SOA formation for the VBS requires the determination of the yields of each volatility bin (volatility distribution of products) and the corresponding enthalpies of vaporization.

The SOA parametrizations for the VBS have been traditionally based on fitting yield measurements (Lane et al., 2008). The major weakness of this approach is that the resulting parametrization is limited to the range of OA concentrations and temperatures of the measurements. In most cases, the concentration range does not include the low concentrations relevant to the atmosphere and usually most of the experiments take place in a relatively narrow temperature range. Pathak et al. (2007a) needed 37 smog chamber experiments at different temperatures (0–45 ºC) and atmospherically relevant concentrations to constrain the α-pinene SOA temperature sensitivity.

A number of approaches has been used to minimize the number of experiments needed to characterize the temperature dependence of the SOA formation. Stanier et al. (2007) developed an experimental technique with which the temperature-controlled

smog chamber could be heated or cooled after the SOA formation moving the system to new equilibrium favoring evaporation or condensation respectively. However, interactions of the SOA with the walls of the system increased the uncertainties of the approach. Stanier et al. (2008) presented an algorithm to fit the smog chamber experiments using several volatility bins. However, the number of experiments needed by the algorithm should cover a wide range of concentrations and temperatures to effectively constrain the stoichiometric mass yields and the effective vaporization enthalpy.

In an effort to cover a wider concentration and temperature range, thermodenuder measurements can be used. The tThermodenuder (TD) is a common instrument developed to characterize the volatility of atmospheric aerosols by heating them and observing the resulting changes in size, mass, optical properties, etc. (Burtscher et al., 2001; Wehner et al., 2002, 2004; An et al., 2007). TDs consist of a heated tube in which the more volatile particle components evaporate followed by a cooling section with activated carbon to avoid vapor recondensation. The mass changes in TDs depend on the initial SOA concentration, the residence time in the heating tube, the vaporization enthalpy, and the mass transfer resistances. The latter areis described by the effective accommodation coefficient thatand has been traditionally used to account for resistances to mass transfer not only at the surface of the particle but also inside the particle. The evaporation rate for most particles is relatively insensitive to its value when this valueit is around one. A typical way of reporting the TD measurements is by calculating the aerosol mass fraction remaining (MFR) at a given temperature after passing through the TD. The MFRs in a range of TD temperatures constitute the thermogram.

In TD applications in the field (Cappa and Jimenez, 2010; Huffman et al., 2009; Lee et al., 2010; Louvaris et al., 2017a) and in the laboratory (Kalberer et al., 2004; Baltensperger et al., 2005; An et al., 2007; Lee et al., 2011; Cain et al., 2020) the particles system does not reach equilibrium with the gas phase inside the TD. Therefore, dynamic aerosol evaporation models (Riipinen et al., 2010; Cappa, 2010; Fuentes and McFiggans, 2012) are needed for the interpretation of TD measurements. Karnezi et al. (2014) used the time-dependent evaporation model of Riipinen et al. (2010) to calculate the OA volatility distribution, vaporization enthalpy, and mass accommodation coefficient from TD measurements. The authors showed that a simple error minimization approach may not be appropriate for such systems as very similar

thermograms can be obtained for multiple combinations of different parameters. For this reason, their approach estimates an ensemble of "good" solutions, from which the best estimate and the corresponding uncertainties are derived.

Grieshop et al. (2009) suggested the combination of TD and isothermal dilution to constrain the volatility distribution of SOA. Karnezi et al. (2014) proposed an algorithm to include both ~~two~~ types of measurements. The authors concluded that the combination of the two types of measurements can better constrain the OA volatility than each set separately. Louvaris et al. (2017b) and Cain et al. (2020) applied this algorithm to cooking OA (COA) and SOA, respectively. Louvaris et al. (2017b) showed that the use of only TD measurements led to overestimation of the SVOC fraction of COA, while the use of TD and isothermal dilution data reduces the uncertainty of the volatility distribution and ~~of~~ the effective vaporization enthalpy. Cain et al. (2020) ~~obtained~~ conducted ~~experimentally~~ TD and isothermal dilution ~~measurements~~ experiments for α-pinene and cyclohexene ozonolysis SOA. The SOA in these two systems had similar thermograms, but different areograms. When only thermograms were used in the model, the volatility distributions were quite similar. However, the addition of areograms revealed that α-pinene ozonolysis SOA consists mostly of low-volatility organic compounds (LVOCs) and the cyclohexene ozonolysis SOA consists mostly of SVOCs.

To constrain the volatility product distribution of SOA and its effective vaporization enthalpy, we combine TD and isothermal dilution experiments with the SOA yield measurements. We extend here the algorithm of Karnezi et al. (2014) by introducing additional inputs (SOA yields) and ~~by~~also providing additional outputs (uncertainty of estimated yields in relevant atmospheric conditions). The algorithm is tested with "pseudo-experimental" data generated from the use of models simulating the corresponding measurement processes, ~~therefore~~so the true parameters are known. The results of the "pseudo-experiments" are corrupted so that they include experimental errors.

2. Model Description

2.1. SOA Formation

Gas-phase oxidation of VOCs involves a large number of reactions and produces a large number of products that can condense in the particulate phase. Depending on their

136 effective saturation concentration, they can be represented in the 1D-VBS framework

137 by

$$VOC + oxidant \rightarrow \alpha_1 P_1 + \alpha_2 P_2 + ... + \alpha_n P_n + volatile\ products \qquad (1)$$
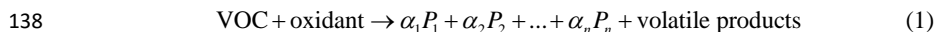
139 where n is the number of the surrogate compounds (volatility bins in the VBS), P_i is the

140 surrogate product in the i-th volatility bin and α_i is the corresponding stoichiometric

141 mass yield. The total SOA mass yield can be then calculated as:

$$Y \equiv \frac{C_{OA}}{\Delta VOC} = \sum_{i}^{n} \frac{\alpha_i}{1 + \left(C_i^* / C_{OA} \right)} \qquad (2)$$

143 where C_{OA} is the total SOA concentration, ΔVOC is the consumed concentration of the

144 VOC and C_i^* is the effective saturation concentration of compound i. This yield

145 equation is an extension of the two-product model by Odum et al. (1996) replacing their

146 semi-empirical partitioning coefficients with the assumption of a pseudo-ideal solution

147 (Strader et al., 1999). This model assumes that the system has reached equilibrium when

148 the yield was measured and that the differences in molecular weights are small.

149   The effective saturation concentrations at different temperatures are given by

150 the Clausius-Clapeyron equation:

$$C_i^* \left(T \right) = C_i^* \left(T_{ref} \right) \frac{T_{ref}}{T} \exp\left[\frac{\Delta H_{vap,i}}{R} \left(\frac{1}{T_{ref}} - \frac{1}{T} \right) \right] \qquad (3)$$

152 where T_{ref} is the reference temperature in which the reference effective saturation

153 concentration is defined (298 K in this work), and $\Delta H_{vap,i}$ is the enthalpy of vaporization

154 of surrogate compound i.

155

156 **2.2. Thermodenuder Model**

157 The time-dependent evaporation of SOA in the TD used ~~is described~~ in this work is

158 described by the dynamic mass transfer model of Riipinen et al. (2010). The evolution

159 of the total particle mass, m_p, and the gas phase concentration of the compound i, C_i are

160 given by:

$$\frac{dm_p}{dt} = -\sum_{i=1}^{n} I_i \qquad (4)$$

$$\frac{dC_i}{dt} = I_i N_{tot} \qquad (5)$$

163 where n is the number of surrogate compounds, N_{tot} is the total number concentration

164 of particles (assuming monodisperse aerosol population) and I_i is the mass flux of

Commented [ОП18]: Reviewer #3, Comment #18

165 compound i from the gas to the particulate phase for each particle calculated by
166 (Seinfeld and Pandis, 2016):

$$I_i = \frac{2\pi d_\mathrm{p} M_i \beta_{\mathrm{m}i} D_i}{R T_\mathrm{TD}} \left(p_i - p_i^0 \right) \tag{6}$$

168 where d_p is the particle diameter, R is the ideal gas constant, M_i is the molecular weight
169 of compound i, D_i is the diffusion coefficient of compound i in the gas phase at
170 temperature T_TD, p_i and p_i^0 are the partial vapor pressures of i far away from the particle
171 and at particle surface, respectively, and $\beta_{\mathrm{m}i}$ is a factor for the correction of kinetic and
172 transition regime effects (Fuchs and Sutugin, 1970):

$$\beta_{\mathrm{m}i} = \frac{1 + Kn_i}{1 + \left(\frac{4}{3\alpha_{\mathrm{m}i}} + 0.377 \right) Kn_i + \frac{4}{3\alpha_{\mathrm{m}i}} Kn_i} \tag{7}$$

174 where Kn_i is the Knudsen number of compound i, and $\alpha_{\mathrm{m}i}$ is the mass accommodation
175 coefficient of compound i on the particles. The partial vapor pressure of compound i at
176 the particle surface is given by:

$$p_i^0 = x_{\mathrm{m}i} \frac{C_i^* R T}{M_i} \exp\left(\frac{4 M_i \sigma}{R T_\mathrm{TD} \rho d_\mathrm{p}} \right) \tag{8}$$

178 where $x_{\mathrm{m}i}$ is the mass fraction of compound i in the particulate phase, C_i^* is the effective
179 saturation concentration, σ is the surface tension (assumed 0.05 N m^{-1} in our
180 simulations), T_TD is the particle temperature assumed to be the same as in the TD, and
181 ρ is the particle density. The effective saturation concentrations at different TD
182 temperatures are given by Eq. (3).
183 Processes other than organic aerosol evaporation may affect the TD
184 measurements. For example, thermal decomposition may accelerate the transfer of
185 organic compounds from the particulate to the gas phase and may lead ~~Because aerosol~~
186 ~~particles are heated at relatively high temperatures in TD, thermal decomposition is a~~
187 ~~potential process preceding evaporation leading~~ to overestimation of the volatility of
188 especially the least volatile components of the SOA (Epstein et al., 2010; Saha and
189 Grieshop, 2016; Stark et al., 2017). However, the corresponding parameters for the
190 SVOCs and the more volatile LVOCs ~~and the SVOCs~~ that are important for
191 atmospheric SOA modeling should be a lot less uncertain given that they are measured
192 in relatively low TD temperatures. The use of isothermal dilution measurements may
193 also help identify cases in which the model does not include a process (e.g., thermal

6

decomposition) that dominates the behavior of the aerosol during heating. In this case, one expects that the overall algorithm will have difficulties reproducing all measurements (yields, isothermal dilution, and evaporation in the TD).

2.3. Isothermal Dilution Model

In isothermal dilution experiments, a SOA sample is injected in a reactor filled with clean air at room temperature. The concentrations of both the gas and particulate phase components are lowered due to dilution leading the system out of equilibrium. The evaporation of SOA as a result of isothermal dilution is also described by equations (3)-(8) (Karnezi et al., 2014), but the temperature is equal to 298 K. Evaporation in a dilution chamber depends on the initial SOA mass, time, and the α_m, but not on ΔH_{vap} as the particles evaporate without a change in temperature.

The dilution ratio is an important parameter ~~in dilution processes~~, varying typically from 10 to 20 in SOA ~~smog chamber~~ experiments (Cain et al., 2020). Low dilution ratios result in little evaporation and little signal to be explored by the parameter estimation algorithm. High dilution ratios lead to very low initial concentrations in the dilution chamber and a lot of noise in the subsequent evaporation measurements.

3. Algorithm for the Estimation of VBS Parameters

The algorithm of Karnezi et al. (2014) was first extended to include an SOA partitioning model described by Equations. (1) – (3) together with the TD and isothermal dilution models in order to estimate the volatility product distribution, vaporization enthalpy and accommodation coefficient. We discretized the domain of the parameters and simulated all combinations of stoichiometric mass yields (α_i), ΔH_{vap}, and α_m. The yields α_i were allowed to vary from 0.0 to 0.8, with values of 0.0, 0.05, 0.1, 0.15, 0.2, 0.3, 0.4, 0.6, and 0.8. The user of the algorithm can specify an upper limit for the sum of the yields to reduce the number of the potential solutions that the algorithm will test. C~~For oxidation products in the volatility bins less than 10^3 µg m^{-3}, c~~Combinations with sum of the yields exceeding 1.0 were excluded from the analysis originally. The sensitivity of our results to setting the upper limit of the sum of the yields equal to 2 is examined in Section 4.6. For a 4-product system there are 3,153 and for 6-product system 66,636 acceptable combinations. The values used for ΔH_{vap} were from 20 to 200 kJ mol^{-1} with a step of 20, and for α_m, the values used were 0.001, 0.01, 0.1, and 1. As a result 126,120

Commented [ОП20]: Reviewer #2, Comment #12

Commented [ОП21]: Reviewer #2, Comment #24

Commented [ОП22]: Reviewer #2, Comment #4

228 simulations are needed (computational time of about 15 h in an office PC) for a 4-

229 product VBS and 2,665,440 for a 6-product solution.

230   For each simulation and each type of measurement, we calculated the

231 *normalized mean square error* (NMSE) defined as

$$\text{NMSE} = \frac{\sum_{i=1}^{N_O}\left(P_i - O_i\right)^2}{\sum_{i=1}^{N_O} O_i} \tag{9}$$

232

233 where O_i represents the ith observed value (corresponding to a specific SOA

234 concentration for yield measurements or temperature for TD, or time for isothermal

235 dilution), P_i the corresponding model-predicted value, and N_O is the total number of

236 observations from each type of measurement. For each simulation (denoted as s), the

237 overall error was calculated by assuming equal weight to the set of yield, TD, and

238 dilution measurements and summing the corresponding errors:

239 $$E_s = \text{NMSE}_{Y,s} + \text{NMSE}_{\text{TD},s} + \text{NMSE}_{\text{Dil},s} \tag{10}$$

240   The parameter combinations for which the overall error E_s is less than 5% are

241 identified. The best solution is then calculated by averaging these solutions using the

242 inverse error E_s as a weighting factor. The solutions that are closer to the measurements

243 have higher weight. Therefore, for every combination of α_i, ΔH_{vap}, and α_m the algorithm

244 calculates one overall *NMSE* following Eq. (10) and all data points for each solution

245 get the same weighting factor. More specifically the best estimate $\bar{x}$ is given by:

$$\bar{x} = \frac{\sum_{k}^{N} x_k \frac{1}{E_k}}{\sum_{k}^{N} \frac{1}{E_k}} \tag{11}$$

246

247 where x_k is the estimated value of a property (mass yield of a volatility bin, effective

248 vaporization enthalpy, or effective accommodation coefficient) and N is the number of

249 combinations with error below the threshold value. The uncertainty range of the

250 parameters is estimated by calculating the standard deviation (σ):

$$\sigma = \sqrt{\frac{\sum_{k}^{N}\left[\left(x_k - \bar{x}\right)^2 \cdot \frac{1}{E_k}\right]}{\sum_{k}^{N} \frac{1}{E_k}}} \tag{12}$$

251

252 following Karnezi et al. (2014).

8

4. Testing of the Algorithm

4.1. Generation of Data for Evaluation

In order to evaluate the algorithm, we generated data using the output of SOA formation, thermodenuder and isothermal dilution models described in Section 2 for systems with known volatility distribution of the products, and properties. Then, these data were "corrupted" with random errors to represent the "noise" observed in laboratory measurements for yields, thermograms, and areograms. As a result, there is no set of model parameters that can reproduce all the "measurements". The yields were corrupted based on the variability of laboratory measurements of Pathak et al. (2007a), by assuming a normal distribution and standard deviation (σ_Y) given by:

$$\sigma_Y = 0.1 Y_{\text{true}} + 0.02 \tag{13}$$

where Y_{true} are the correct yields.

For TD, the errors were calculated by assuming a normal distribution and the standard deviation (σ_{TD}) suggested by Karnezi et al. (2014):

$$\sigma_{\text{TD}} = 0.51 MFR_{\text{TD,true}} - 0.5 \left(MFR_{\text{TD,true}} \right)^2 \tag{14}$$

where $MFR_{\text{TD,true}}$ are the correct MFR values for each TD temperature.

For dilution, the errors were calculated by assuming a uniform distribution and standard deviation (σ_{Dil}) suggested by Karnezi et al. (2014):

$$\sigma_{\text{Dil}} = 0.05 \, MFR_{\text{Dil,true}} + 0.03 \tag{15}$$

where $MFR_{\text{Dil,true}}$ are the correct MFR values for isothermal dilution.

Based on the above methodology, we generated "pseudo-measurements" of yield, TD, and isothermal dilution for different SOA systems. The parameters used to produce the pseudo-experimental data are summarized in Table S1. The "experimental" conditions assumed for the TD and isothermal dilution measurements are shown in Table S2.

In "Experiment" A, we test the performance of the algorithm against α-pinene ozonolysis data and examine the effect of TD and isothermal dilution data. For "Experiment" A, the "true" values were taken from the parameterization derived by Pathak et al. (2007b) for the ozonolysis of α-pinene at low NO_x, dark and low RH conditions. So Therefore, these results are good fits of the measurements analyzed in that study. The parametrization was derived assuming a 4-volatility bin system with saturation concentrations ranging from 1 to 10^3 μg m^{-3}. The effective vaporization

286 enthalpy estimated in that study was equal to 30 kJ mol^{-1}. Because the effective
287 accommodation coefficient was not part of the Pathak et al. (2007b) parametrization,
288 we assumed a value of 0.5 in this work. We used a small number of yield measurements
289 at atmospherically relevant SOA concentrations of 1, 5, 10, 20 and 40 μg m^{-3} (Fig. 1).
290 For this SOA system, the yield at 40 μg m^{-3} did not exceed 20%. The thermogram
291 includes ten MFR data points in the temperature range of 20 to 200 ^{o}C. For the highest
292 temperature, more than 70% of the SOA mass was evaporated. The areogram shows
293 that the correspondent SOA evaporated almost by 70 % in the first 0.5 h and more than
294 90% in less than 3 h.

295   For "Experiment" B, the "true" values were taken from the alternative
296 parametrization proposed by Pathak et al. (2007b) for the same oxidation system as
297 described before. This time, the authors used a 7-volatility bin system with saturation
298 concentrations ranging from 10^{-2} to 10^{4} μg m^{-3} in their parametrization. The effective
299 vaporization enthalpy of the parametrization was 30 kJ mol^{-1}, while for the
300 accommodation coefficient we assumed again a value of 0.5. The yield, TD and
301 isothermal dilution "measurements" of Experiment B are generated in the same SOA
302 mass concentration, temperature, and dilution time range as in the previous pseudo-
303 experiment (Fig. 2).

304   For "Experiment" C, the "true" values were based on the parameterization of
305 the SOA formed during α-humulene ozonolysis by Sippial et al. (2022). The authors
306 measured high SOA yields for α-humulene in the main smog chamber (~70% at 60 μg
307 m^{-3}), and their corresponding thermogram suggested that the SOA particles fully
308 evaporated at 150 ^{o}C, while the areogram showed modest (20%) evaporation in the
309 dilution chamber after 3 hours. A 4-volatility bin set with saturation concentrations
310 ranging from 10^{-2} to 10 μg m^{-3} was used in that study to fit the measurements. The
311 stoichiometric coefficients of the three least volatile bins (10^{-2}, 10^{-1} and 1 μg m^{-3}) were
312 around 0.1 and for the most volatile (10 μg m^{-3}) 0.25. The vaporization enthalpy was
313 115 kJ mol^{-1} and the accommodation coefficient was 0.01 (Table S1). We assumed five
314 yield "measurements" in the SOA concentration range of 1 to 100 μg m^{-3} with yield
315 values as high as 65 % at 100 μg m^{-3} (Fig. 3). The corresponding thermogram consisted
316 of 10 data and the particles fully evaporated at TD temperatures higher than 150 ^{o}C.
317 The areogram consisted of 17 data points and only 20 % of the SOA evaporated in the
318 dilution chamber.

319

4.2. Parameter Estimation for "Experiments" A, B, and C

We explored the performance of the algorithm for different choices of the number of volatility bins, the range of saturation concentrations, and the range of SOA mass concentration range in the yield measurements. For each test, the "true" and the estimated properties are summarized in Table 1.

We evaluated the performance of our parameter estimation algorithm comparing its predictions both against the "measurements" and ~~also against~~ the "truth" defined as the predictions of the original parameterization. In both comparisons, *mean normalized error* (MNE) (Emery et al., 2017) was used as the evaluation metric because it has a simpler physical meaning ~~and provides a more comprehensive understanding for the reader~~ than NMSE.

For the evaluation against the "measurements", the MNE_{M} was defined as

$$MNE_{\mathrm{M}} = \frac{100}{N_O} \sum_{i=1}^{N_O} \frac{\left| EST_i - O_i \right|}{O_i} \tag{16}$$

where EST_i is the estimated by the algorithm value and corresponds to a specific measured point O_i.

For the evaluation against the "truth", which includes conditions (e.g., temperatures or concentrations) for which there are no available measurements, the MNE_{T} was defined as:

$$MNE_{\mathrm{T}} = \frac{100}{N_d} \sum_{j=1}^{N_d} \frac{\left| EST_j - TR_j \right|}{TR_j} \tag{17}$$

where EST and TR are the estimated and the "true" values respectively. N_d is the total number of data points included in calculations and depends on the selected discretization of the corresponding dependent variable (e.g., SOA concentration, TD temperature, and dilution time). We used a linear discretization for the SOA concentrations (from 0.01 to 50 μg m^{-3} with a step of 0.01) and the TD temperatures (20 to 200 ºC with a step of 5 ºC but ~~including TD MFR values greater than zero~~ excluding zero MFR values to avoid the division by zero). For the dilution time, the sampling timestep was not constant. ~~w~~We used a higher resolution for the first 0.5 hour (step of 2 min), in which the evaporation is usually faster, and a lower resolution afterwards ~~then~~ (step of 10 min) ~~up to 3 hours~~.

349   Finally, we used the average relative standard deviation (*ARSD*) as a metric to
350   quantify the uncertainty of the estimates (range of good solutions) using the same
351   discretization as in the *MNE*$_T$ metric. The *ARSD* is given by:

352
$$ARSD = \frac{100}{N_d} \sum_{j=1}^{N_d} \frac{\sigma_j}{EST_j} \qquad (18)$$

353   where σ_j is the standard deviation for data point *j*.

354

4.2.1 Parameter Estimation for "Experiment" A

356   In Test A1, we applied the algorithm in the same range of saturation concentrations and
357   with the same number of volatility bins as these used to produce the "experimental"
358   data. The upper bin (10^3 µg m^{-3}) exceeded the maximum SOA concentration (40 µg
359   m^{-3}) in the measurement range by one order of magnitude.
360   Figure 1 depicts the estimated and the range of the ensemble of best solutions
361   for the three types of "measurements" for Test A1. There were 148 number of "good"
362   solutions under the 5% threshold were 148 out of the 126,120 simulations (Table S3).
363   Tand the density distribution of the solutions isare depictedshown in Figure S1. The

364   performance of the model for the yields at 25 °C was quite encouraging with a small
365   tendency of overprediction for SOA higher than 10 µg m^{-3}. The *MNE*$_M$ of the model for
366   the SOA yield "measurements" (given by Eq. 16) was equal to 25% (Table 2). The
367   corresponding discrepancy between the true parameterization and the measurements
368   (due to the measurement error that we introduced) was 21.2% (Table 2). This indicates
369   that a significant part of the algorithm error can be explained by the uncertainty
370   introduced in the measurements.
371   Our algorithm can be used to calculate the SOA yield at different concentrations
372   and temperatures. The yields were calculated in the atmospherically relevant range of
373   0–50 µg m^{-3} SOA concentration and at four temperatures (5, 15, 25, and 35 °C) using
374   the true parameter values and the estimated parameters of Test A1 (Fig. 1-a-d). At 25

375   °C (Fig. 1c), the estimated yield curve is in good agreement with the "true" yield curve
376   for SOA concentrations lower than 6 µg m^{-3} (error of 8% at 6 µg m^{-3}), but the
377   discrepancies increase at higher concentrations (error of 23% at 50 µg m^{-3}). The average
378   *MNE*$_T$ error between the true parametrization and the estimated values (given by Eq.
379   17) was equal to 17.3% for yields at 25 °C (Table 3). The uncertainties, as expected,
380   are larger at lower temperatures. However, the *MNE*$_T$ error (estimated yields compared

12

381 to the true value) remains less than 25% (Table 3) even at 5 $^{\circ}$C, quite far from the

382 measurement temperature. ~~MNE_T and MNE_M were used to quantify the performance of~~

383 ~~the algorithm.~~ Both MNE_T and MNE_M were quite close to the introduced experimental

384 error. Their difference can be~~was~~ explained by both the "noise" introduced to the

385 "measurements" that affects MNE_M and the higher number of points used to calculate

386 MNE_T.

387 ~~At this point, we should point out that~~ T~~t~~he SOA model used in this work

388 assumes that the stoichiometric coefficients (α_i) are temperature independent.

389 Therefore, processes, such as formation of highly oxygenated organic molecules

390 (HOMs) ~~formation~~ and oligomerization which are expected to be ~~highly temperature~~

391 ~~dependent~~temperature dependent (Quéléver et al., 2019; Gao et al., 2022), are not

392 described by our algorithm.

393 The algorithm provides a range of "good" estimates in addition to the best

394 estimate. The range can be defined by the lower and upper SOA yield limits of the

395 ensemble of the good solutions at each point. At 25 $^{\circ}$C, the yield range increased, as

396 expected, at higher concentrations (yield range of 0.05 at 1 μg m^{-3} to 0.17 at 50 μg

397 m^{-3}). The average relative standard deviation (*ARSD* of the estimated yields defined by

398 Eq. 18) was equal to 26% (Table 4) for the 25 $^{\circ}$C case. For the rest of the temperatures,

399 the *ARSD* increased for the lower temperatures, ranging from 24% at 35 $^{\circ}$C to 35% at

400 5 $^{\circ}$C (Table 4) and including in all cases the true solution.

401 For the TD (Fig. 1e), the model reproduced well the correspondent thermogram

402 with low errors compared to the "measurements" with an error MNE_M of 7% (Table 2).

403 The error MNE_T compared to the "true" values was 5.5% (Table 3). The error of the

404 TD "measurements" compared to the true values was equal to 7.6% (Table 2).

405 Therefore, the error of the proposed algorithm is quite similar to the experimental error.

406 The error introduced into the "measurements" was transferred, as expected, to the error

407 metrics of the algorithm.

408 For the isothermal dilution (Fig. 1f), the algorithm did reasonably well for the

409 first 30 minutes and then the evaporation was slightly underpredicted leading to an error

410 MNE_M of 16.7% (Table 2). This MNE_M value was roughly two times higher than the

411 corresponding error between the dilution measurements and the true parametrization

412 (Table 2). The error between the estimated and the "true" values MNE_T was 19%. The

413 *ARSD* of 24% (Table 4) was sufficient to include the true solution.

13

Commented [ОП35]: Reviewer #3, Comment #5

Commented [ОП36]: Reviewer #2, Comment #11

Commented [ОП37]: Reviewer #2, Comment #16

Commented [ОП38]: Reviewer #2, Comment #16

The estimated volatility distribution of the products and the effective vaporization enthalpy and accommodation coefficient using the three types of measurements can be seen in Figure 4 and Table 1. The estimated volatility distribution of the products was in a good agreement with the "true" values (α_i absolute difference of 0.01 at 1 µg m^{-3}, 0.03 at 10 µg m^{-3}, 0.07 at 10^2 µg m^{-3}, and 0.04 at 10^3 µg m^{-3}) and the estimated uncertainties contained the correct values. There is a large uncertainty range for the two higher volatility bins (standard deviation higher than 0.13) indicating that yield values at higher ~~a wider range of~~ SOA concentrations would be needed to better constrain these volatility bins. The relative error of the estimated ΔH_{vap} is 10%. The estimated accommodation coefficient was 0.17 compared to a true value of 0.5. The estimated uncertainty for the effective accommodation was almost one order of magnitude (from 0.06 to 0.51) indicating the difficulty of constraining this parameter when it is close to unity and thus the resistances to mass transfer are small.

4.2.2 Parameter Estimation for "Experiment" B

In this section, we ~~used~~ analyze the pseudo-experimental data of Experiment B, which were obtained from the parametrization of the same smog chamber results used in Experiment A~~experiment as described before~~, but ~~for an SOA system~~ with more components and a much wider range of volatilities including LVOCs, SVOCs and IVOCs (10^{-2}–10^4 µg m^{-3}). In Test B1, the algorithm was applied using a 4-bin VBS with saturation concentrations ranging from 1 to 10^3 µg ____m^{-3}. ~~This range is narrower than the actual range used to obtain the pseudo measurements of Experiment B.~~ In this test, we attempted to model the behavior of the system with a narrower volatility range than the real one. The upper limit of the saturation concentration range that we tested did not exceed the 10^3 µg m^{-3} because Experiment B took place in moderate SOA concentration levels (up to 40 µg m^{-3}), which means that it is practically impossible to constrain the 10^4 µg m^{-3} or ~~more~~ higher volatile bins.

Figure 2 shows the results of the fitting for the three types of "measurements" in this experiment. There were 82 ~~number of~~ "good" solutions under the 5% threshold ~~were 82~~ out of 126,120 simulations (Table S3) and the density of the solutions are shown in Figure S2. At 25 °C, the model performance for the yields is encouraging (MNE_M=20.6%). This is again pretty close to the measurement error (20.5%). By comparing the estimated and the "true" yield curves at 25 °C, the error MNE_T is now 14%. The error increases to 31% at 5 °C, far from the available measurements. This is

Commented [ОП39]: Reviewer #2, Comment #27

Commented [ОП40]: Reviewer #2, Comment #15

Commented [ОП41]: Reviewer #2, Comment #5 Reviewer #3, Comment #4

Commented [ОП42]: Reviewer #2, Comments #6 and #7

Commented [ОП43]: Reviewer #2, Comments #19 and #20

14

448 reflected also in the increase of the uncertainty of our estimates with the *ARSD*
449 increasing from 17% at 35 °C to 37% at 5 °C (Table 4). Once more the uncertainty
450 range estimated by the algorithm includes the true values.

451 Both "measured" and "true" thermogram were well captured by the best
452 estimate (MNE_M of 6% and MNE_T of 4%) with an uncertainty *ARSD* of 20.5%. The
453 evaporation in the dilution chamber was a little underestimated for the first 2 h, but then
454 it was slightly overpredicted. The MNE_T for the areogram was 13.3% and the true values
455 were included within the range of the estimates (*ARSD* of 18%).

456 Figure 5 shows the results of Test B1 for the volatility distribution of the
457 products. The "true" stoichiometric coefficient for the 1 μg m^{-3} bin was overestimated
458 by 0.01 by the algorithm. This overestimation actually corresponds to the total material
459 of the 10^{-2} and 10^{-1} μg m^{-3} bins of the "true" system. This indicates that the algorithm
460 places the material of the two lowest bins that are not part of the solution to the bin with
461 the lower volatility. For the 10 μg m^{-3} and 10^2 μg m^{-3} bins, the relative errors between
462 the estimated and "true" were 58% and 277% respectively (Table S4~~3~~), while for the
463 10^3 μg m^{-3} bin, the relative error was 10 %. The ΔH_{vap} was predicted accurately (error
464 of only 4%), while α_m was underpredicted (0.1 instead of 0.5). The model compensates
465 for the missing volatility bins by increasing the material in the 10^2 μg m^{-3} bin and by
466 decreasing the accommodation coefficient.

> **Commented [ОП44]:** Reviewer #2, Comment #5

467 The results of Test B1 suggest that the mismatch between the actual SOA
468 volatility distribution and the range used for the fits can introduce significant errors in
469 the retrieved distribution for individual volatility bins. However, despite these
470 problems, the yields predicted by the derived parameterizations have a much lower

> **Commented [ОП45]:** Reviewer #3, Comment #20

471 error than the volatility distribution. This is a valuable insight for the strengths and
472 weaknesses of this and other similar SOA parameter estimation algorithms.

473

4.2.3 Parameter Estimation for "Experiment" C

475 In Test C1, we obtained the best fits for the pseudo-measurements of Experiment C by
476 applying the algorithm in the same range of saturation concentrations and with the same
477 number of volatility bins (4 volatility bins in the 10^{-2}–10^1 μg m^{-3} saturation
478 concentration range) as the true volatility distribution.

479 Figure 3 shows the results of the fitting for the three types of "measurements".
480 There were 3,479 ~~number of~~ "good" solutions under the 5% threshold ~~were 3,479 out~~
481 of the 126,120 simulations (Table S3). T~~and t~~he density distribution of the solutions

15

isare shown in Figure S3. The best estimate for the SOA yields at 25 ℃ was in a good

agreement with the "measurements" (MNE_M=6.3%) and the "true" values (MNE_T=9.6%). For the rest of the temperatures, there was a decreasing trend of the error as the temperature decreased varying from 15.5% at 35 ℃ to 6.2% at 5 ℃. A similar decreasing trend was observed for the uncertainty $ARSD$ of the estimates which varied from 23% at 35 ℃ to 15% at 5 ℃. This behavior is the opposite from what we observed in the previous tests, in which both errors and uncertainties increased at lower temperatures. However, the changes in both the error and the uncertainty are small (change of around 7% between the upper and lower temperature for both metrics), indicating that this system is less temperature-sensitive in this temperature range than the previous ones.

The performance of the algorithm was satisfactory compared to the TD "measurements" (MNE_M=12.9%). The corresponding error of the algorithm for the true values (MNE_T) was 4.4% for temperatures up to 110 ℃ and equal to 10.6% for the lower values at higher temperatures. According to Figure 3, the evaporation due to dilution was initially overestimated for the first 30 min, but then underestimated (highest MFR discrepancy of 0.05) and there is a high uncertainty range of the corresponding estimates (MFR range of 0.46 at 3 h). However, the low dilution values resulted in low relative errors (MNE_M of 3.5% and MNE_T of 2.7%).

Figure 6 shows that the highest relative errors were calculated for the 10^{-1} and 10^0 µg m^{-3} bins (23% and 33% respectively), and smaller relative errors for the other two bins (less than 13%). The uncertainties were almost of the same magnitude for all bins with standard deviations ranging from 0.09 to 0.13. The performance of the model was good for the ΔH_{vap} (relative error of 7%), but with high uncertainty for α_m.

4.3. Effect of the Volatility Range

In in this section, we explore the performance of the algorithm for different choices of the number of volatility bins and the range of saturation concentrations. The analysis of the results of Test B1 has already quantified the effects of using a narrower volatility distribution in the parameter estimation algorithm than the one of the investigated SOA system. Additional sensitivity tests are performed here for all cases.

In Test A2, we used 3 volatility bins covering the $1–10^2$ µg m^{-3} saturation concentration range instead of the 4 bins used in Test A1 and covering the 10^3 µg m^{-3} material. The narrower assumed volatility range had a very small effect on the estimated

516   yields at all temperatures (Table 3 and Fig. S4+) compared to Test A1. The change in

517   MNE_T ranged from 3% at 5 ºC to 0.3% at 35 ºC. Minor changes were detected in the

518   predicted thermogram (change of 0.8%) and areogram (change of 0.5%) as well. The

519   uncertainty of the yield estimates increased by less than 2.5% at all temperatures. The

520   estimated volatility distribution of the SOA products of Test A2 changed by less than

521   5% in the two lower bins. The material in the 10^2 μg m^{-3} increased by 15% to account

522   for the SOA of higher volatility that could not be included otherwise in the estimated

523   distribution. The estimated ΔH_{vap} was in this case 32 kJ mol^{-1} (2.7% decrease) and the

524   α_m decreased by 12% with respect to Test A1.

525   In Test A3, we shifted the assumed 4-bin volatility distribution by one order of

526   magnitude to lower values (from 1–1000 μg m^{-3} in Test A1 to 0.1–100 μg m^{-3} in Test

527   A3), covering in that way the 0.1–100 μg m^{-3} saturation concentration range. In this

528   case, the algorithm distributed exactly the same material to the 1, 10 and 100 μg m^{-3}

529   volatility bins as in Test A2, and it predicted correctly zero SOA in the 0.1 μg m^{-3} bin

530   (Table 1). The ΔH_{vap} and α_m estimated values were also unchanged with respect to Test

531   A2. This in turn, led to the same estimated yields at different temperatures (no change

532   in the error between the two tests).

533   In Test C2, we applied the algorithm against the Experiment C "measurements"

534   using a 4-volatility bin system in the 1 to 10^3 μg m^{-3} range, that is two orders of

535   magnitude higher than the actual range of the "true" values. Figure 7 shows the results

536   of the fitting for the three types of "measurements". Despite the significant mismatch

537   of the volatility distributions the MNE_M increased by only 2.3% for the estimated SOA

538   yields. The error for the TD measurements increased by 20% while it actually decreased

539   a little (1.2%) for the dilution data. The errors compared to the true values increased by

540   less than 3% for the temperature range 15–35 ºC while it increased by 12% at 5 ºC.

541   These results suggest that the estimated yields are quite robust in this case to the

542   assumed volatility range. The major effect of the mismatch in volatility ranges was

543   evident in the predicted thermogram with overestimation of the MFR for the 60–120

544   ºC temperature range and underprediction in higher temperatures. The increase in

545   MNE_T for the TD MFR was 17.2% (Table 3). The change in the predicted areogram

546   was marginal and led to a small increase of MNE_T (error increase by 0.7%) (Table 3).

547   The algorithm underestimated again the α_m (0.004 instead of 0.01) but also recognized

548   the high uncertainty of the corresponding estimate. The algorithm distributed

549   significant material to the 1 μg m^{-3} bin (3.6 times higher than the actual), in an effort to

Commented [ОП48]: Reviewer #3, Comment #21

550　account for the absence of the 10^{-2} and 10^{-1} μg m^{-3} bins. The ΔH_{vap} was underestimated
551　with an error of 21%.

552　　　　The results of the above tests indicate that a mismatch between the true and
553　assumed volatility ranges of the SOA increases in general the estimation error but the
554　increase is small to modest. This is reassuring for the robustness of the proposed
555　algorithm.

556

557　**4.4. Effect of Measurements at ~~Hh~~igh SOA Levels**

558　During the last decade there has been a significant shift of the performed SOA smog
559　chamber towards lower SOA concentrations. This is needed to increase the accuracy at
560　the ambient concentration levels. The high SOA concentration experiments that once
561　represented the majority of the performed experiments are becoming increasingly rare.
562　In this paragraph we examine the value of these high concentration experiments for the
563　estimation of SOA yields at ambient conditions.

564　　　　To examine the effect of "measurements" at SOA levels much higher than the
565　atmospheric ones, we included an extra yield measurement at 200 μg m^{-3} in the yield
566　data of Experiments A and B. In Test A4 and B2, we applied the algorithm once again
567　against the three types of "measurements" by using a 4-volatility bin system with
568　saturation concentrations ranging from 1 to 10^3 μg m^{-3}.

569　　　　In Test A4, the additional experiment at high SOA concentration led to an MNE_T
570　of 15.7% for the yields at 25 °C (Table 3 and Fig. S5~~2~~), which is by 1.6% lower than
571　that without this experiment in Test A1. The improvement was more significant at
572　lower temperatures e.g., the MNE_T at 5 °C was reduced from 24.4% to 20.4%. The
573　reduction in the $ARSD$ for the SOA yields ranged from 3.8% at 5 °C to 0.9% at 35 °C
574　(Table 4). Figure 8 depicts the results of the model for the yields and the volatility
575　distribution of the products for Test A4. The accuracy of the predicted volatility
576　distribution increased especially for the higher volatility material. For example, the
577　error for the 10^2 μg m^{-3} bin was reduced from 41% in Test A1 to 6% in this case (Table
578　S3). Minor changes in the errors were detected for the ΔH_{vap} and α_m between the two
579　tests (3% increase and 6% decrease respectively).

580　　　　Similar to Test A4, in Test B2 we added a yield measurement at 200 μg m^{-3} in
581　the Experiment B set of "measurements". Figure 9 depicts the results of the model for
582　the SOA yields at 25 °C and the estimated volatility distribution of the products. The
583　use of the additional data point led to a reduction of the NME_T from 13.9% in Test B1

18

584 to 9% in Test B2 at 25 °C (Table 3). Similar reductions in the NME_T were observed for

585 the other temperatures, with the highest one observed at 5 °C (lower error by 7%)

586 (Figure 10). The reduction in the $ARSD$ for the estimated yields ranged from 3.3% at 5

587 °C to 1.2% at 35 °C (Table 4). Minor changes were observed for the estimated

588 thermogram (Fig. S6~~3~~) (change in the NME_T of 1.5%) and the uncertainty of the

589 estimates (change in the $ARSD$ of 2.5%). The error in the estimated areogram was also

590 small but in this case the error increased by 5%. The additional data point helped

591 decrease the errors for the estimated mass of the more volatile SOA products (Fig. 9)

592 and especially for the 10^2 μg m^{-3} bin. The ΔH_{vap} and α_m estimated values were only

593 slightly affected by the additional measurement.

594 By comparing the results Tests B1 and B2 with ~~the~~ Case ~~True~~ A, one would

595 expect that the retrieved volatility distribution of the products will be quite similar.

596 T~~However, t~~he differences present are due to a large extent to the different random

597 experimental errors introduced in~~to~~ the two sets of "measurements" for~~in~~ Experiments

598 A and B ~~were different~~. A second reason for the differences is that ~~In addition, although~~

599 ~~the~~ parametrizations of the two "Experiments" by Pathak et al. (2007b) even if they

600 were derived from the same ~~realistic~~ smog chamber experiments have some differences.

601 As a result ~~,~~the ~~correspond~~ "true" yields, thermogram, and areogram in Cases A and B

602 are not exactly the same ~~turned to be relatively different~~ (see Figs. 1 and 2).

Commented [ОП49]: Reviewer #2, Comment #6

603 These results suggest that an additional yield measurement at high SOA can

604 lead to a substantial reduction of the error for the estimated yields at low temperatures

605 (Fig. 10) and also a better estimation of the SOA products with higher volatility (10^2

606 and 10^3 μg m^{-3}). These products may contribute little to the SOA concentration at 25

607 °C, but their reactions (aging) could lead to significant additional SOA in later stages.

608

609 **4.5. Significance of Each Type of Measurement~~s for the~~ Parametrization**

Commented [ОП50]: Reviewer #2, Comments #3 and #9 Reviewer #3, Comment #2

610 To quantify the effect of each type of measurement for the parameter estimation~~into~~

611 ~~parametrization~~ and their subsequent effect on the estimated SOA yields, we repeated

612 ~~the~~ tests A1, B1, and C1 withholding one set of measurements. More specifically, we

613 used the algorithm providing it the following combination of measurements: ~~without~~

614 ~~providing as input the type of measurements concerned. Therefore, we repeated all the~~

615 ~~previous tests for the following three combinations of measurements:~~ TD and

isothermal dilution, SOA yields and isothermal dilution, and finally SOA yields and TD.

~~We started with the~~The use of only the ~~combination of~~ TD and isothermal dilution data corresponds for all practical purposes to the previous algorithm of ~~, which is practically the same as that of~~ Karnezi et al. (2014) which has been the starting point of this work. In Test A1, the absence of the yield measurements led to a significant deterioration of the ability of the algorithm to estimate SOA yields at all temperatures and concentrations (Fig. S7). The SOA yield error of the algorithm in the 5–35 ºC temperature range increased from 14-24% (when all measurements are provided) to approximately 100% (Table S5). The corresponding uncertainty range also increased by a factor of 4-6 (Table S6). Similar results were obtained in the other tests.

Figure S8 shows the volatility distribution of the products, ΔH_{vap} and α_m in Test A1. High discrepancies and uncertainties were observed for the estimated stoichiometric coefficients (α_i), with an increase in the relative error by a factor of ~~about~~ 3 ~~and~~ 4 for the 1~~10^0~~ and 10^1 µg m^{-3} bins ~~respectively~~ (Table S7) ~~when~~ compar~~ing~~ed to the ~~with the~~ case when~~of~~ all three types of measurements are used.

Figures S9 and S10 show~~s~~ the results of the algorithm for Test A1 when only the SOA yields and isothermal dilution measurements are provided as inputs to the algorithm. In this case~~Test A1,~~ the algorithm ~~had difficulties at~~cannot constrain~~ing~~ well the ΔH_{vap} (relative error of almost 270% with respect to the true value) as a result of ~~not providing~~the missing TD measurements. This led to significant increase in the MNE_T for the estimated yields when moving far from the ~~measurement~~ temperature of the measurements (MNE of 65% at 15 ºC and 122% at 5 ºC).

Figures S11 and S12 show~~s~~ the results of the algorithm for Test A1 when only yield and TD measurements are provided as inputs. In this case, there was a significant reduction in the error for the ΔH_{vap} respect to the previous case (from 270% to 50%), but it was still much higher than the 10% error when all three types of measurements were used. This led to better agreement between the true and estimated yields at lower temperatures (MNE_T of 23% and $ARSD$ of 44%).

When comparing TD/Dilution, Yields/Dilution, and Yields/TD results, the Yield/TD combination gave the best results out of the three pairs. The isothermal dilution measurements are the least valuable of the three because only a relatively small fraction of the SOA evaporates and therefore the information provided is relatively limited and focuses on the more volatile components of the particles. Also, TD

20

measurements are important to constrain well ΔH_{vap} and allow the more accurate extrapolation of the results to other temperatures. also provides information for the volatility distribution of the OA. However, our results suggest that the combination of the three types of measurements does need to a major improvement over either the TD/Dilution approach or the Yield/TD approach.

4.6. Sensitivity ~~Tests~~ to ~~a Different Choice of~~ the Upper Limit of the Sum of Product Yields

The maximum sum of the VBS product yields is one of the parameters that the user of the algorithm chooses. In the analysis so far a value of 1 had been selected to reduce the computational cost of the algorithm. Selected tests were repeated using a maximum sum of 2 to quantify the effects of this choice on the estimated parameters and more importantly on the SOA yields predicted by the parameterization. ~~To test the sensitivity of our results we have repeated certain tests using 2.0 (instead of 1.0 as described in Section 3) as an upper limit for the sum of the yields.~~ For a 4-product system there are 9,191 product yield combinations and~~.~~ ~~c~~Considering the discretization of ΔH_{vap} and α_m, this leads to a total of 367,120 simulations (Table S3).

The increase in the ~~$\Sigma(\alpha_s)$~~ upper limit of the sum of the yields ~~from 1.0 to 2.0~~ led to an increase in the "good"~~accepted~~ solutions in Tests A1, A4, B1, B2, and C2. The additional~~new~~ solutions had different yields mostly in~~affected~~ the 10^3 μg m^{-3} bin. This led to ~~leading to~~ an increase of the mass yield of this bin by 37% in Test A1, 47% in Test B1, and 29% in Test C2 (Table S8). ~~T~~However, ~~t~~the uncertainties were even higher showing once again the difficulty to constrain the IVOC~~s~~ range where there are no SOA measurements at very high SOA concentrations. The new parametrizations had a minor effect on the estimated yields at different temperatures with maximum change in the MNE_T found at 5 °C (change of 1.8% in Test A1 and 1.2% in Test B2) and much smaller otherwise (Table S9). Therefore, the use of the higher upper limit has an effect on the estimate of the 10^3 μg m^{-3} bin which is quite uncertain in all cases, but has a minor effect on the predicted SOA yields at ambient conditions.

5. Conclusions

An algorithm was developed to estimate VBS parameters for SOA formation combining yield measurements from atmospheric simulation chambers with thermodenuder and isothermal dilution measurements chambers. An additional feature

684 of this approach is that the algorithm estimates the uncertainty of the predicted SOA
685 yields for different SOA concentrations and temperatures, assisting in this way in the
686 design of future experiments.

687 The algorithm was evaluated against pseudo-experimental data for SOA
688 systems with known properties. The algorithm performed quite well at reproducing the
689 SOA yields at atmospherically relevant concentrations and temperatures with errors
690 less than 20% for practically all cases. This was the case even at temperatures as low
691 as 5 °C and also when the volatility range used for the parameter estimation was
692 narrower than that of the simulated SOA system. One should note that this error was
693 quite similar in most cases to the experimental error assumed in the construction of the
694 "measurement" datasets.

695 The errors in the retrieved SOA volatility distributions were in general higher
696 than those of the SOA yields. This is due to a large extent to the existence of multiple
697 solutions that can result in similar yields. The accuracy of the estimated mass fractions
698 of the more volatile SOA components improved when an additional yield measurement
699 at high SOA (e.g., at 200 $\mu g\ m^{-3}$). The addition of this measurement also improved the
700 estimated yields at low temperatures. This therefore suggests that data points at high
701 SOA concentrations should also be obtained experimentally, together with the data
702 points at atmospherically relevant atmospheric SOA levels.

703 In all cases the algorithm results in good estimates of the effective evaporation
704 enthalpy. On the other hand, the estimates of the effective accommodation coefficient
705 are usually quite uncertain. The effect of the mass accommodation coefficient on the
706 measured quantities is relatively small compared to the other parameters (volatility
707 distribution, effective evaporation enthalpy) making it difficult to constrain. This
708 conclusion is consistent with the results of Karnezi et al. (2021). The addition of the
709 SOA yields to the inputs does not make much of a difference, because these are not
710 affected by the accommodation coefficient.

711 The approach combining yield, TD (thermograms), and isothermal dilution
712 (areograms) measurements is recommended for future parametrizations of SOA
713 formation.

714 The use of the results of these experiments that have been designed for the
715 measurement of SOA yields to other applications (e.g., new particle formation) should
716 be performeddone with caution. Our results indicate that the derived parameterizations
717 are able to predict the SOA yields under different atmospheric conditions with errors

Commented [ОП52]: Reviewer #3, Comment #3

718 of around 20% or less, but the derived volatility distributions can be quite uncertain.
719 These uncertainties are higher for the tails of the distribution (the low volatility and the
720 intermediate volatility organic compounds). Different experiments should be probably
721 performed for the derivation of the VBS distribution if for example on is interested in
722 new particle formation and therefore the low volatility organics ~~in this case~~ focusing on
723 low SOA concentration levels and the least volatile SOA components.

Commented [OⲚ53]: Reviewer #2, Comment #8

6. Code and data availability

The code and simulation results are available upon request (spyros@chemeng.upatras.gr).

7. Supplementary information

8. Author contribution

PU, and SNP designed the research. PU developed the final model code. AD developed a first version of the code and performed preliminary feasibility tests. DS and SNP designed the experiments for the α-humulene ozonolysis and DS carried them out. PU performed the simulations, the formal analysis, and wrote the original draft. Paper review and editing was performed by SNP.

9. Competing interests

The authors declare that they have no conflict of interest.

10. Financial support

11. References

An, W. J., Pathak, R. K., Lee, B. H. and Pandis, S. N.: Aerosol volatility measurement using an improved thermodenuder: Application to secondary organic aerosol, J. Aerosol Sci., 38, 305–314, doi:10.1016/j.jaerosci.2006.12.002, 2007.

Baltensperger, U., Kalberer, M., Dommen, J., Paulsen, D., Alfarra, M. R., Coe, H., Fisseha, R., Gascho, A., Gysel, M., Nyeki, S., Sax, M., Steinbacher, M., Prevot, A. S. H., Sjögren, S., Weingartner, E. and Zenobi, R.: Secondary organic aerosols from anthropogenic and biogenic precursors, Faraday Discuss., 130, 265–278, doi:10.1039/b417367h, 2005.

Burtscher, H., Baltensperger, U., Bukowiecki, N., Cohn, P., Hüglin, C., Mohr, M., Matter, U., Nyeki, S., Schmatloch, V., Streit, N. and Weingartner, E.: Separation of volatile and non-volatile aerosol fractions by thermodesorption: Instrumental development and applications, J. Aerosol Sci., 32, 427–442, doi:10.1016/S0021-8502(00)00089-6, 2001.

Cain, K. P., Karnezi, E. and Pandis, S. N.: Challenges in determining atmospheric organic aerosol volatility distributions using thermal evaporation techniques, Aerosol Sci. Technol., 54, 941–957, doi:10.1080/02786826.2020.1748172, 2020.

Cappa, C. D.: A model of aerosol evaporation kinetics in a thermodenuder, Atmos. Meas. Tech., 3, 579–592, doi:10.5194/amt-3-579-2010, 2010.

Cappa, C. D. and Jimenez, J. L.: Quantitative estimates of the volatility of ambient organic aerosol, Atmos. Chem. Phys., 10, 5409–5424, doi:10.5194/acp-10-5409-2010, 2010.

Donahue, N. M., Robinson, A. L., Stanier, C. O. and Pandis, S. N.: Coupled partitioning, dilution, and chemical aging of semivolatile organics, Environ. Sci. Technol., 40, 2635–2643, doi:10.1021/es052297c, 2006.

Emery, C., Liu, Z., Russell, A. G., Odman, M. T., Yarwood, G., and Kumar, N.: Recommendations on statistics and benchmarks to assess photochemical model performance, J. Air Waste Manag. Assoc., 67, 582–598, ~~https://doi.org/~~doi:10.1080/10962247.2016.1265027, 2017.

Epstein, S. A., Riipinen, I. and Donahue, N. M.: A semiempirical correlation between enthalpy of vaporization and saturation concentration for organic aerosol, Environ. Sci. Technol., 44, 743–748, doi:10.1021/es902497z, 2010.

Fuchs, N. A. and Sutugin, A. G.: Highly Dispersed Aerosols, Ann Arbor Science Publishers, Ann Arbor, London., 1970.

24

783   Fuentes, E. and McFiggans, G.: A modeling approach to evaluate the uncertainty in

784   estimating the evaporation behaviour and volatility of organic aerosols, Atmos.

785   Meas. Tech., 5, 735–757, doi:10.5194/amt-5-735-2012, 2012.

786   Gao, L., Song, J., Mohr, C., Huang, W., Vallon, M., Jiang, F., Leisner, T., and Saathoff,

787   H.: Kinetics, SOA yields, and chemical composition of secondary organic aerosol

788   from β-caryophyllene ozonolysis with and without nitrogen oxides between 213

789   and 313 K, Atmos. Chem. Phys., 22, 6001–6020, doi:10.5194/acp-22-6001-2022,

790   2022

791   Grieshop, A. P., Miracolo, M. A., Donahue, N. M. and Robinson, A. L.: Constraining

792   the volatility distribution and gas-particle partitioning of combustion aerosols using

793   isothermal dilution and thermodenuder measurements, Environ. Sci. Technol., 43,

794   4750–4756, doi:10.1021/es8032378, 2009.

795   Huffman, J. A., Docherty, K. S., Mohr, C., Cubison, M. J., Ulbrich, I. M., Ziemann, P.

796   J., Onasch, T. B. and Jimenez, J. L.: Chemically-resolved volatility measurements

797   of organic aerosol from different sources, Environ. Sci. Technol., 43, 5351–5357,

798   doi:10.1021/es803539d, 2009.

799   IPCC: Climate Change 2013: The Physical Science Basis. Contribution of Working

800   Group I to the Fifth Assessment Report of the Intergovernmental Panel on Climate

801   Change, Cambridge., 2013.IPCC: Climate Change 2021: The Physical Science

802   Basis. Contribution of Working Group I to the Sixth Assessment Report of the

803   Intergovernmental Panel on Climate Change, [Masson-Delmotte, V., Zhai, P.,

804   Pirani, A., Connors, S.L., Péan, C., Berger, S., Caud, N., Chen, Y., Goldfarb, L.,

805   Gomis, M.I., Huang, M., Leitzell, K., Lonnoy, E., Matthews, J.B.R., Maycock,

806   T.K., Waterfield, T., Yelekçi, O., Yu, R., and Zhou, B. (eds.)]. Cambridge

807   University Press, Cambridge, United Kingdom and New York, NY, USA, In press,

808   doi:10.1017/9781009157896, 2021.

809   Kalberer, M., Paulsen, D., Sax, M., Steinbacher, M., Dommen, J., Prevot, A. S. H.,

810   Fisseha, R., Weingartner, E., Frankevich, V., Zenobi, R. and Baltensperger, U.:

811   Identification of polymers as major components of atmospheric organic aerosols,

812   Science, 303, 1659–1662, doi:10.1126/science.1092185, 2004.

813   Kanakidou, M., Seinfeld, J. H., Pandis, S. N., Barnes, I., Dentener, F. J., Facchini, M.

814   C., Van Dingenen, R., Ervens, B., Nenes, A., Nielsen, C. J., Swietlicki, E., Putaud,

815   J. P., Balkanski, Y., Fuzzi, S., Horth, J., Moortgat, G. K., Winterhalter, R., Myhre,

816   C. E. L., Tsigaridis, K., Vignati, E., Stephanou, E. G. and Wilson, J.: Organic

Commented [ОП55]: Reviewer #2, Comment #11

Commented [ОП56]: Reviewer #2, Comment #22

817   aerosol and global climate modelling: A review, Atmos. Chem. Phys., 5, 1053–
818   1123, doi:10.5194/acp-5-1053-2005, 2005.

819 Karnezi, E., Riipinen, I. and Pandis, S. N.: Measuring the atmospheric organic aerosol
820   volatility distribution: A theoretical analysis, Atmos. Meas. Tech., 7, 2953–2965,
821   doi:10.5194/amt-7-2953-2014, 2014.

822 Lane, T. E., Donahue, N. M. and Pandis, S. N.: Effect of NO_x on secondary organic
823   aerosol   concentrations,   Environ.   Sci.   Technol.,   42,   6022–6027,
824   doi:10.1021/es703225a, 2008.

825 Lee, B. H., Kostenidou, E., Hildebrandt, L., Riipinen, I., Engelhart, G. J., Mohr, C.,
826   Decarlo, P. F., Mihalopoulos, N., Prevot, A. S. H., Baltensperger, U. and Pandis, S.
827   N.: Measurement of the ambient organic aerosol volatility distribution: Application
828   during the Finokalia Aerosol Measurement Experiment (FAME-2008), Atmos.
829   Chem. Phys., 10, 12149–12160, doi:10.5194/acp-10-12149-2010, 2010.

830 Lee, B. H., Pierce, J. R., Engelhart, G. J. and Pandis, S. N.: Volatility of secondary
831   organic aerosol from the ozonolysis of monoterpenes, Atmos. Environ., 45, 2443–
832   2452, doi:10.1016/j.atmosenv.2011.02.004, 2011.

833 Lim, S. S., Vos, T., Flaxman, A. D., Danaei, G., Shibuya, K., Adair-Rohani, H., Amann,
834   M., Anderson, H. R., Andrews, K. G., Aryee, M., Atkinson, C., Bacchus, L. J.,
835   Bahalim, A. N., Balakrishnan, K., Balmes, J., Barker-Collo, S., Baxter, A., Bell, M.
836   L., Blore, J. D., Blyth, F., Bonner, C., Borges, G., Bourne, R., Boussinesq, M.,
837   Brauer, M., Brooks, P., Bruce, N. G., Brunekreef, B., Bryan-Hancock, C., Bucello,
838   C., Buchbinder, R., Bull, F., Burnett, R. T., Byers, T. E., Calabria, B., Carapetis, J.,
839   Carnahan, E., Chafe, Z., Charlson, F., Chen, H., Chen, J. S., Cheng, A. T. A., Child,
840   J. C., Cohen, A., Colson, K. E., Cowie, B. C., Darby, S., Darling, S., Davis, A.,
841   Degenhardt, L., Dentener, F., Des Jarlais, D. C., Devries, K., Dherani, M., Ding, E.
842   L., Dorsey, E. R., Driscoll, T., Edmond, K., Ali, S. E., Engell, R. E., Erwin, P. J.,
843   Fahimi, S., Falder, G., Farzadfar, F., Ferrari, A., Finucane, M. M., Flaxman, S.,
844   Fowkes, F. G. R., Freedman, G., Freeman, M. K., Gakidou, E., Ghosh, S.,
845   Giovannucci, E., Gmel, G., Graham, K., Grainger, R., Grant, B., Gunnell, D.,
846   Gutierrez, H. R., Hall, W., Hoek, H. W., Hogan, A., Hosgood, H. D., Hoy, D., Hu,
847   H., Hubbell, B. J., Hutchings, S. J., Ibeanusi, S. E., Jacklyn, G. L., Jasrasaria, R.,
848   Jonas, J. B., Kan, H., Kanis, J. A., Kassebaum, N., Kawakami, N., Khang, Y. H.,
849   Khatibzadeh, S., Khoo, J. P., Kok, C., et al.: A comparative risk assessment of
850   burden of disease and injury attributable to 67 risk factors and risk factor clusters

851 in 21 regions, 1990-2010: A systematic analysis for the Global Burden of Disease
852 Study 2010, Lancet, 380, 2224–2260, doi:10.1016/S0140-6736(12)61766-8, 2012.

853 Louvaris, E. E., Florou, K., Karnezi, E., Papanastasiou, D. K., Gkatzelis, G. I. and
854 Pandis, S. N.: Volatility of source apportioned wintertime organic aerosol in the
855 city of Athens, Atmos. Environ., 158, 138–147, doi:10.1016/j.atmosenv.2017.
856 03.042, 2017a.

857 Louvaris, E. E., Karnezi, E., Kostenidou, E., Kaltsonoudis, C. and Pandis, S. N.:
858 Estimation of the volatility distribution of organic aerosol combining
859 thermodenuder and isothermal dilution measurements, Atmos. Meas. Tech., 10,
860 3909–3918, doi:10.5194/amt-10-3909-2017, 2017b.

861 Odum, J. R., Hoffmann, T., Bowman, F., Collins, D., Flagan, R. C. and Seinfeld, J. H.:
862 Gas/particle partitioning and secondary organic aerosol yields, Environ. Sci.
863 Technol., 30, 2580–2585, doi:10.1021/es950943+, 1996.

864 Pankow, J. F.: An absorption model of gas/particle partitioning of organic compounds
865 in the atmosphere, Atmos. Environ., 28, 185–188, doi:10.1016/1352-
866 2310(94)90093-0, 1994a.

867 Pankow, J. F.: An absorption model of the gas/aerosol partitioning involved in the
868 formation of secondary organic aerosol, Atmos. Environ., 28, 189–193,
869 doi:10.1016/1352-2310(94)90094-9, 1994b.

870 Pathak, R. K., Stanier, C. O., Donahue, N. M. and Pandis, S. N.: Ozonolysis of α-pinene
871 at atmospherically relevant concentrations: Temperature dependence of aerosol
872 mass fractions (yields), J. Geophys. Res., 112, 1–8, doi:10.1029/2006JD007436,
873 2007a.

874 Pathak, R. K., Presto, A. A., Lane, T. E., Stanier, C. O., Donahue, N. M. and Pandis, S.
875 N.: Ozonolysis of α-pinene: Parameterization of secondary organic aerosol mass
876 fraction, Atmos. Chem. Phys., 7, 3811–3821, doi:10.5194/acp-7-3811-2007,
877 2007b.

878 Pope, C. A. and Dockery, D. W.: Health effects of fine particulate air pollution: Lines
879 that connect, J. Air Waste Manag. Assoc., 56, 709–742,
880 doi:10.1080/10473289.2006.10464485, 2006.

881 Quéléver, L. L. J., Kristensen, K., Normann Jensen, L., Rosati, B., Teiwes, R.,
882 Daellenbach, K. R., Peräkylä, O., Roldin, P., Bossi, R., Pedersen, H. B., Glasius,
883 M., Bilde, M., and Ehn, M.: Effect of temperature on the formation of highly

oxygenated organic molecules (HOMs) from alpha-pinene ozonolysis, Atmos. Chem. Phys., 19, 7609–7625, doi:10.5194/acp-19-7609-2019, 2019.

Riipinen, I., Pierce, J. R., Donahue, N. M. and Pandis, S. N.: Equilibration time scales of organic aerosol inside thermodenuders: Evaporation kinetics versus thermodynamics, Atmos. Environ., 44, 597–607, doi:10.1016/j.atmosenv. 2009.11.022, 2010.

Saha, P. K. and Grieshop, A. P.: Exploring dDivergent vVolatility pProperties from yYield and tThermodenuder mMeasurements of sSecondary oOrganic aAerosol from α-pPinene oOzonolysis, Environ. Sci. Technol., 50, 5740–5749, doi:10.1021/acs.est.6b00303, 2016.

Seinfeld, J. H. and Pandis, S. N.: Atmospheric Chemistry and Physics: From Air Pollution to Climate Change, Third., John Wiley & Sons, Hoboken, New Jersey., 2016.

Sippial, D., Uruci, P., Kostenidou, E. and Pandis, S. N.: Formation of secondary organic aerosol during the dark-ozonolysis of α-humulene, Env. Sci. Atmos.submitted for publication, doi: 10.1039/d2ea00181k2023.

Stanier, C. O., Pathak, R. K. and Pandis, S. N.: Measurements of the volatility of aerosols from α-pinene ozonolysis, Environ. Sci. Technol., 41, 2756–2763, doi:10.1021/es0519280, 2007.

Stanier, C. O., Donahue, N. and Pandis, S. N.: Parameterization of secondary organic aerosol mass fractions from smog chamber data, Atmos. Environ., 42, 2276–2299, doi:10.1016/j.atmosenv.2007.12.042, 2008.

Stark, H., Yatavelli, R. L. N., Thompson, S. L., Kang, H., Krechmer, J. E., Kimmel, J. R., Palm, B. B., Hu, W., Hayes, P. L., Day, D. A., Campuzano-Jost, P., Canagaratna, M. R., Jayne, J. T., Worsnop, D. R. and Jimenez, J. L.: Impact of tThermal dDecomposition on tThermal dDesorption iInstruments: Advantage of tThermogram aAnalysis for qQuantifying vVolatility dDistributions of oOrganic sSpecies, Environ. Sci. Technol., 51, 8491–8500, doi:10.1021/acs.est.7b00160, 2017.

Strader, R., Lurmann, F. and Pandis, S. N.: Evaluation of secondary organic aerosol formation in winter, Atmos. Environ., 33, 4849–4863, doi:10.1016/S1352-2310(99)00310-6, 1999.

Wehner, B., Philippin, S. and Wiedensohler, A.: Design and calibration of a thermodenuder with an improved heating unit to measure the size-dependent

918   volatile fraction of aerosol particles, J. Aerosol Sci., 33, 1087–1093,
919   doi:10.1016/S0021-8502(02)00056-3, 2002.
920 Zhang, Q., Jimenez, J. L., Canagaratna, M. R., Allan, J. D., Coe, H., Ulbrich, I., Alfarra,
921   M. R., Takami, A., Middlebrook, A. M., Sun, Y. L., Dzepina, K., Dunlea, E.,
922   Docherty, K., DeCarlo, P. F., Salcedo, D., Onasch, T., Jayne, J. T., Miyoshi, T.,
923   Shimono, A., Hatakeyama, S., Takegawa, N., Kondo, Y., Schneider, J., Drewnick,
924   F., Borrmann, S., Weimer, S., Demerjian, K., Williams, P., Bower, K., Bahreini, R.,
925   Cottrell, L., Griffin, R. J., Rautiainen, J., Sun, J. Y., Zhang, Y. M. and Worsnop, D.
926   R.: Ubiquity and dominance of oxygenated species in organic aerosols in
927   anthropogenically-influenced Northern Hemisphere midlatitudes, Geophys. Res.
928   Lett., 34, 1–6, doi:10.1029/2007GL029979, 2007.
929
930
931

Table 1: True and estimated volatility distribution of the products for 8 different tests. The uncertainty of the estimates ($\pm\sigma$) is also included.

TEST	ΔH_{vap} (kJ mol^{-1})	$log(\alpha_m)$	Stoichiometric Coefficients (α_i) at C_i^* (µg m^{-3})						
			10^{-2}	10^{-1}	10^0	10^1	10^2	10^3	10^4
True A	**30**	**-0.30**	**-**	**-**	**0.070**	**0.038**	**0.179**	**0.300**	**-**
A1	32.9±9.6	-0.77±0.47	**-**	**-**	0.059 ±0.022	0.071 ±0.052	0.252 ±0.130	0.255 ±0.191	**-**
A2	32.0±9.8	-0.72±0.45	**-**	-	0.062 ±0.021	0.067 ±0.053	0.286 ±0.132	**-**	**-**
A3	32.0±9.8	-0.72±0.45	**-**	0.000 ±0.000	0.062 ±0.021	0.067 ±0.053	0.286 ±0.132	**-**	**-**
A4	34.0±9.2	-0.70±0.46	**-**	**-**	0.062 ±0.021	0.082 ±0.050	0.191 ±0.084	0.259 ±0.198	**-**
True B	**30**	**-0.30**	**0.001**	**0.012**	**0.037**	**0.088**	**0.099**	**0.250**	**0.800**
B1	33.8±9.2	-0.95±0.21	**-**	**-**	0.052 ±0.011	0.037 ±0.039	0.374 ±0.122	0.226 ±0.176	**-**
B2	36.5±7.6	-0.93±0.26	**-**	**-**	0.050 ±0.000	0.051 ±0.039	0.292 ±0.103	0.234 ±0.196	**-**
True C	**115**	**-2.02**	**0.118**	**0.094**	**0.116**	**0.247**	-	**-**	**-**
C1	104.6±24.0	-1.74±0.97	0.126 ±0.086	0.116 ±0.090	0.154 ±0.116	0.216 ±0.126		-	**-**
C2	91.2±19.2	-2.36±0.83	**-**	-	0.415 ±0.099	0.143 ±0.117	0.137 ±0.113	0.115 ±0.095	**-**

Table 2: The *mean normilized error* (MNE) between the "measurements" and "true" values, and between the "measurements" and the model estimated values for the different tests.

Test	"Measurements" vs "True" [a]			"Measurements" vs Estimated MNE_M [b]		
	Yield	TD	Dilution	Yield	TD	Dilution
A1	21.2	7.6	9.4	25.0	7.0	16.69
A2	21.2	7.6	9.4	25.1	7.1	16.71
A3	21.2	7.6	9.4	25.1	7.1	16.71
A4	17.8	7.6	9.4	22.4	7.1	19.7
B1	20.5	6.9	5.6	20.6	6.0	14.7
B2	18.1	6.9	5.6	19.1	7.8	18.1
C1	8.4	11.6	1.8	6.3	12.9	3.5
C2	8.4	11.6	1.8	8.6	32.4	2.3

[a] Calculated by $\dfrac{100}{N_O}\sum_{i=1}^{N_o}\dfrac{|O_i - TR_i|}{O_i}$.

[b] Calculated by Eq. (16).

Table 3: The *mean normilized error* between the "true" and estimated values (MNE_T) for the different tests.

Test	Yield				TD	Dilution
	5 ºC	15 ºC	25 ºC	35 ºC		
A1	24.4	21.0	17.3	13.8	5.5	19.0
A2	21.4	19.5	16.9	14.1	4.7	18.5
A3	21.4	19.5	16.9	14.1	4.7	18.5
A4	20.4	18.3	15.7	12.9	6.0	22.5
B1	31.3	21.7	13.9	8.7	4.0	13.3
B2	24.4	15.6	9.0	6.4	2.5	18.4
C1	6.2	6.8	9.6	15.5	4.4 (110 ºC)[*] 10.6 (140 ºC)[*]	2.7
C2	18.1	9.6	7.2	11.5	9.0 (110 ºC)[*] 27.8 (140 ºC)[*]	3.4

[*] The errors for TD were calculated up to the denoted temperature in the parenthesis.

Table 4: The average relative standard deviation (*ARSD*) for the different tests.

Test	Yield				TD	Dilution
	5 ºC	15 ºC	25 ºC	35 ºC		
A1	34.6	29.7	26.0	24.2	21.0	23.6
A2	32.1	28.5	25.2	23.3	21.1	23.2
A3	32.1	28.5	25.2	23.3	21.1	23.2
A4	30.8	27.2	24.5	23.3	21.0	22.1
B1	37.1	27.2	20.0	16.9	20.5	18.0
B2	33.8	25.0	18.5	15.7	18.0	15.9
C1	15.0	14.9	16.2	22.9	20.7[*]	16.5
C2	20.1	15.6	14.1	21.3	20.6[*]	9.8

[*] The *ARSD* for the TD MFR values were calculated in the 20–120 ºC temperature range.
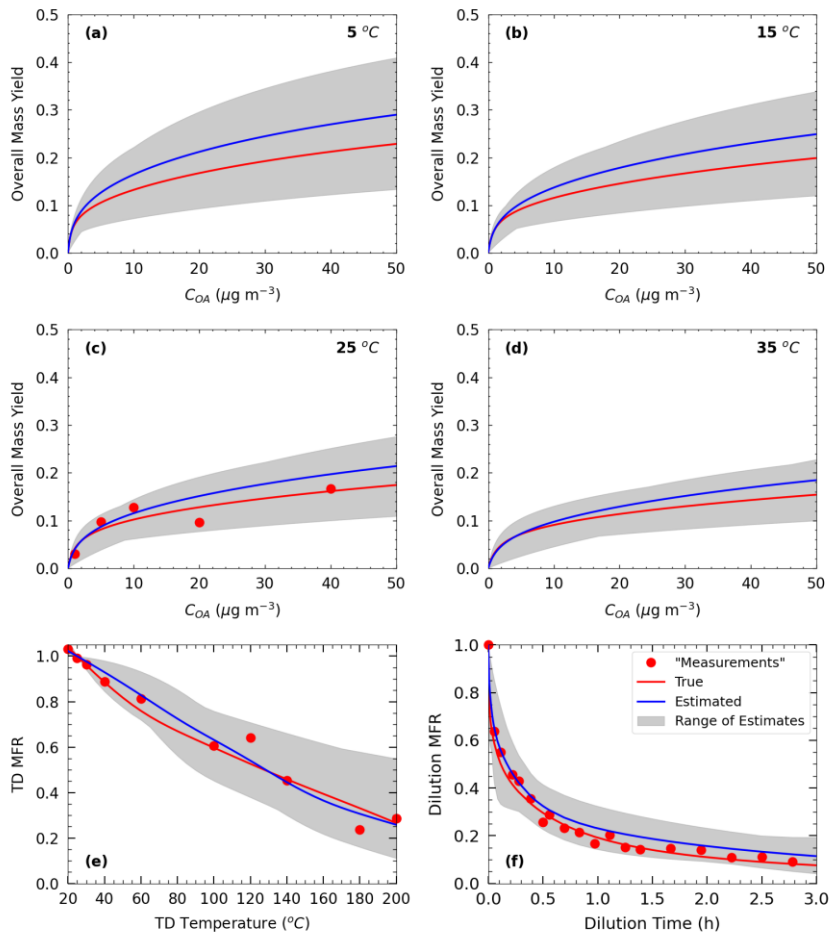
Figure 1: "Measurements" of Test A1 in Experiment A (red dots), true (red line) and estimated (blue line) yields at ~~four temperatures (at~~ (**a**) 5 ºC, (**b**) 15 ºC, (**c**) 25 ºC, and (**d**) 35 ºC), (**e**) TD (thermogram), and (**f**) dilution (areogram) values. The grey area shows the range of good solutions obtained by our algorithm.
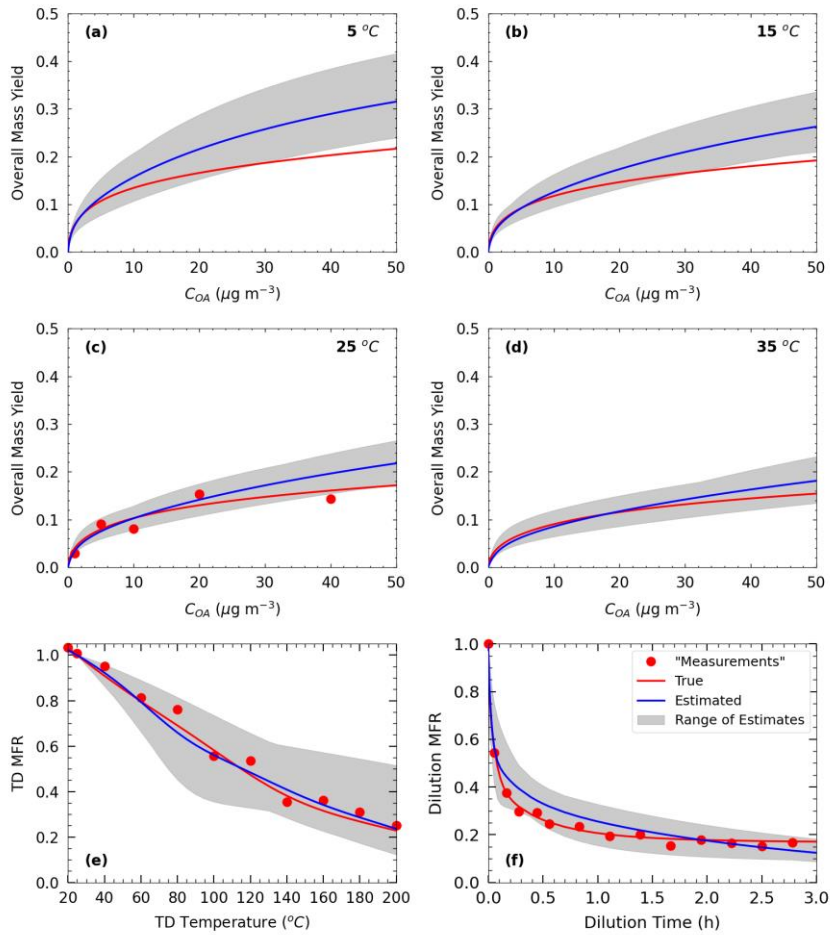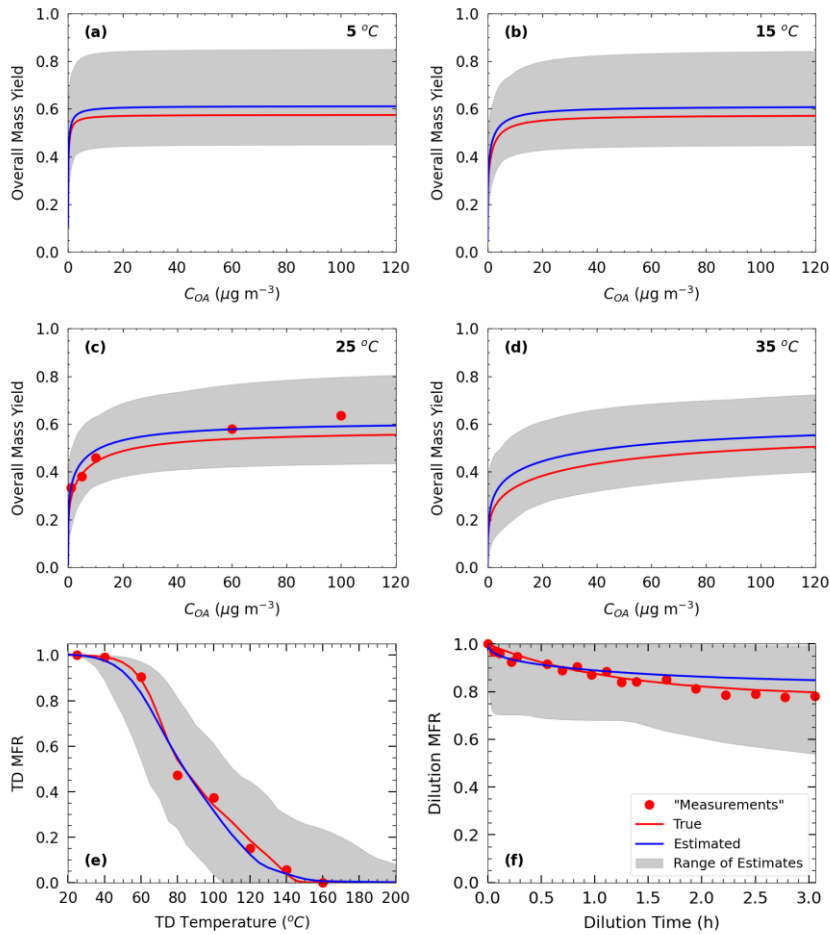
Commented [ОП60]: Reviewer #2, Comment #16

Figure 2: "Measurements" of Test B1 in Experiment B (red dots), true (red line) and estimated (blue line) yields at ~~four temperatures (at~~ **(a)** 5 °C, **(b)** 15 °C, **(c)** 25 °C, and **(d)** 35 °C), **(e)** TD (thermogram), and **(f)** dilution (areogram) values. The grey area shows the range of good solutions.
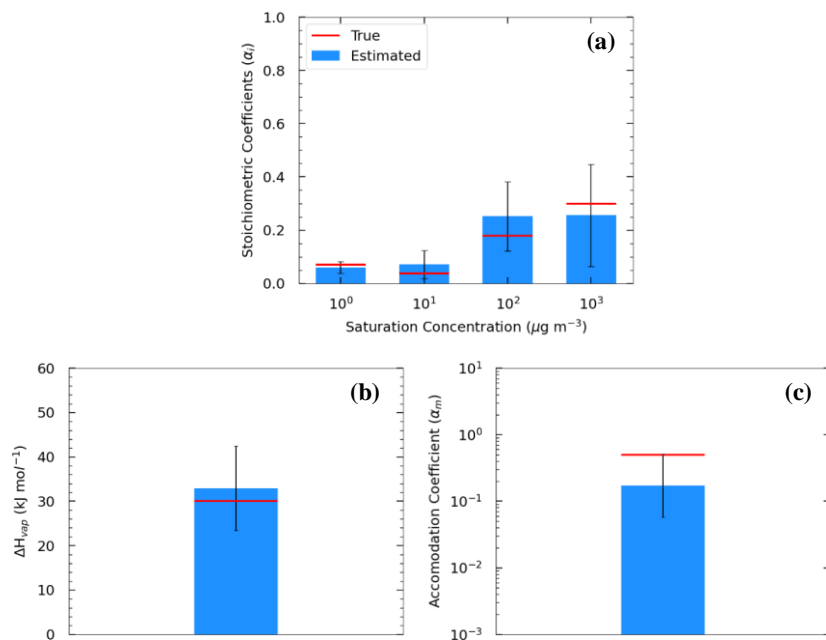
Commented [ОП61]: Reviewer #2, Comment #16

Figure 3: "Measurements" of Test C1 in Experiment C (red dots), true (red line) and estimated (blue line) yields at ~~four temperatures (at~~ (**a**) 5 ^{o}C, (**b**) 15 ^{o}C, (**c**) 25 ^{o}C, and (**d**) 35 ^{o}C), (**e**) TD (thermogram), and (**f**) dilution (areogram) values. The grey area shows the range of good solutions.
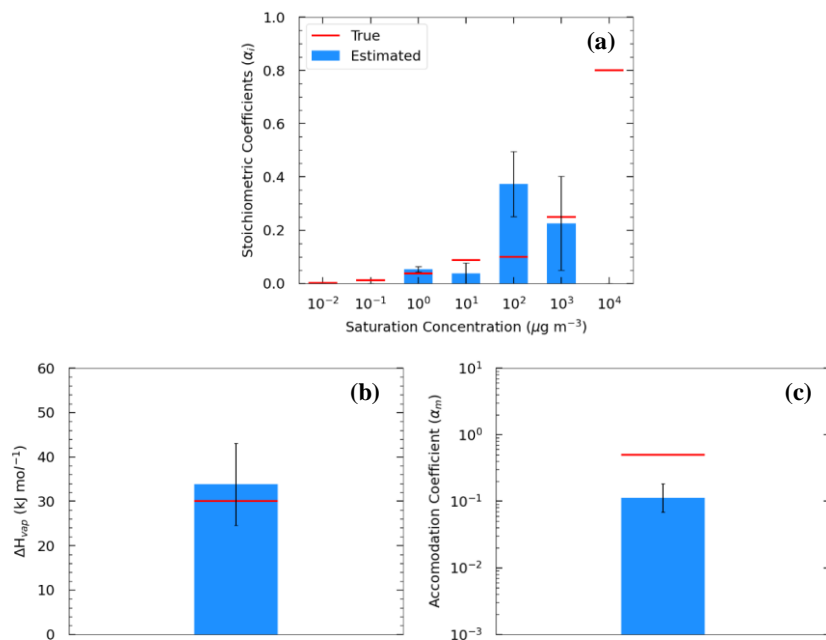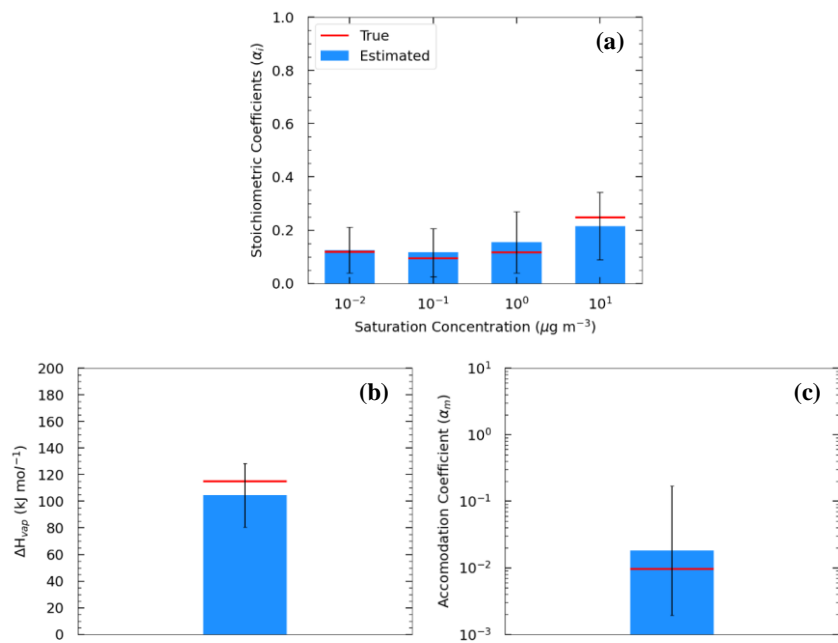
Figure 4. Estimated (bars) and true (red lines) parameter values of Experiment A in Test A1 combining yield, TD, and isothermal dilution measurements for: **(a)** the volatility distribution of the products, **(b)** ΔH_{vap}, and **(c)** α_m. The error bars represent the uncertainty of the estimated values.

Figure 5: Estimated (bars) and true (red lines) parameter values of Experiment B in Test B1 combining yield, TD, and isothermal dilution measurements for: **(a)** the volatility distribution of the products, **(b)** ΔH_{vap}, and **(c)** α_m. The error bars represent the uncertainty of the estimated values.

Figure 6: Estimated (bars) and true (red lines) parameter values of Experiment C in Test C1 combining yield, TD, and isothermal dilution measurements for: **(a)** the volatility distribution of the products, **(b)** ΔH_{vap}, and **(c)** α_m. The error bars represent the uncertainty of the estimated values.
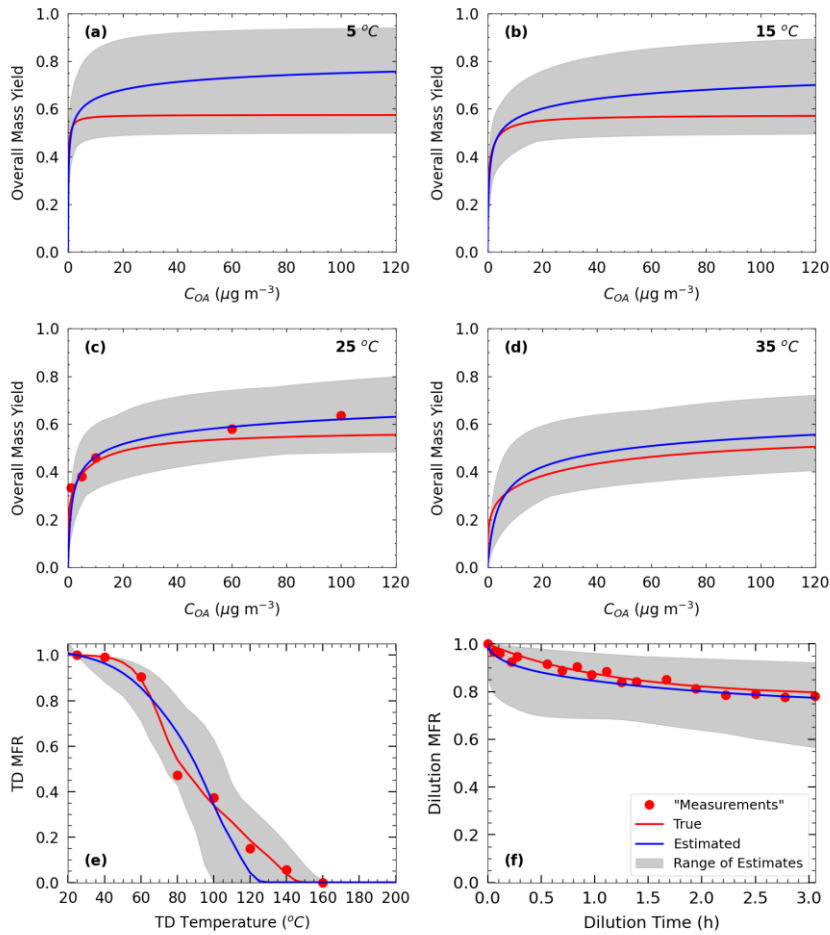
Figure 7: Yields calculated using the "true" parameters of Experiment C (red line) and the estimated (blue line) using the parameters of Test C2 for the following temperatures: (a) 5 °C, (b) 15 °C, (c) 25 °C, and (d) 35 °C. Also shown the (e) thermogram and (f) aerogram. The grey area shows the range of good solutions obtained by our algorithm.

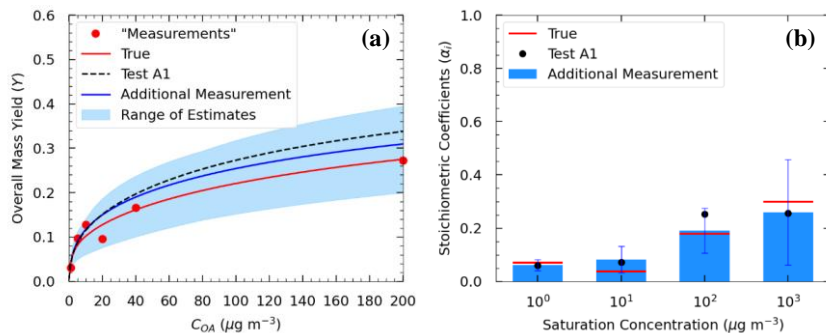Commented [ОП63]: Reviewer #2, Comment #16

Figure 8: (a) True (red line) and estimated (blue line) yields in Test A4, and the "measurements" of Experiment A (red dots) including an additional yield "measurement" at 200 μg m^{-3}. The black dashed line corresponds to the estimated yields in Test A1. **(b)** Estimated volatility distribution of the products (bars) of Test A4 and the true (red lines) parameter values. The black dots correspond to the estimated volatility distribution of the products in Test A1.
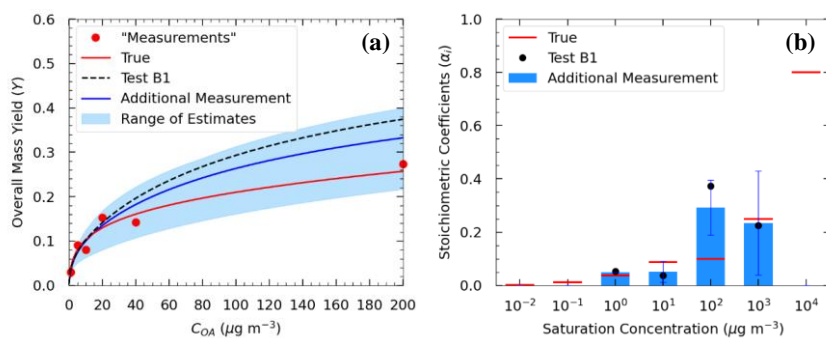

Figure 9: (a) Estimated yields (blue line) in Test B2 and "measurements" of Experiment B (red dots) including an additional yield "measurement" at 200 μg m^{-3}. The black dashed line corresponds to the estimated yields in Test B1. **(b)** Estimated volatility distribution of the products (bars) of Test B2 and the true (red lines) parameter values. The black dots correspond to the estimated volatility distribution of the products in Test B1.
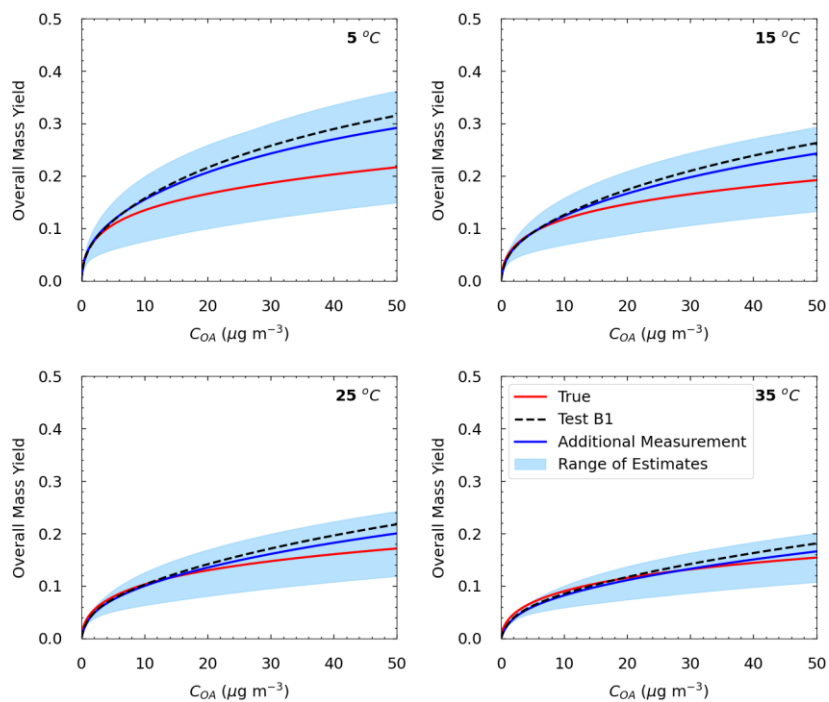
Figure 10: Yields calculated using the "true" parameters of Experiment B (red line) and the estimated (blue line) using the parameters of Test B2 for the following temperatures: 5 °C, 15 °C, 25 °C, and 35 °C. The ~~grey~~ blue area shows the range of good solutions obtained by our algorithm. The black dashed line corresponds to the estimated yields in Test B1.

Commented [ОП66]: Reviewer #2, Comment #17